No Prejudice in Space

R.C. Cotta, J.S. Gainer, J.L. Hewett and T.G. Rizzo[a*]

[a]SLAC National Accelerator Laboratory,
2575 Sand Hill Rd, Menlo Park, CA, 94025, USA

We present a summary of recent results obtained from a scan of the 19-dimensional parameter space of the pMSSM and its implications for dark matter searches.

1. Introduction

Supersymmetry (SUSY) is a leading candidate for a theory of physics beyond the Standard Model. However, it is clear that if SUSY exists, it must be broken. The mechanism by which SUSY is broken is yet unknown and there is a growing list of possible scenarios. In these scenarios, the SUSY spectrum is described by a handful of parameters, generally defined at the SUSY breaking scale; RGE running of sparticle masses and coupling constants yields predictions for the mass spectra and decay patterns of the various sparticles at energy scales relevant for colliders or cosmology. However, these SUSY breaking scenarios are restrictive and predict specific phenomenologies for colliders and cosmology that may not represent the full range of possible SUSY signatures.

Here, we study the MSSM more broadly without assumptions at the high scale. We restrict ourselves to the CP-conserving MSSM (*i.e.*, no new phases) with minimal flavor violation (MFV)[1]. Additionally, we require that the first two generations of sfermions be degenerate as motivated by constraints from flavor physics. We are then left with 19 independent, real, weak-scale, SUSY Lagrangian parameters: the gaugino masses $M_{1,2,3}$, the Higgsino mixing parameter μ, the ratio of the Higgs vevs $\tan\beta$, the mass of the pseudoscalar Higgs boson m_A, and the 10 squared masses of the sfermions ($m_{\tilde{q}1,3}$, $m_{\tilde{u}1,3}$,$m_{\tilde{d}1,3}$,$m_{\tilde{l}1,3}$,and $m_{\tilde{e}1,3}$). We include independent A-terms only for the third generation (A_b, A_t, and A_τ) due to the small Yukawa couplings for the first two generations. This set of 19 parameters has been called the phenomenological MSSM (pMSSM)[2].

To study the pMSSM, we performed a scan over this 19-dimensional parameter space assuming flat priors for the specified ranges[3]: $100\,\mathrm{GeV} \le m_{\tilde{f}} \le 1\,\mathrm{TeV}$; $50\,\mathrm{GeV} \le |M_{1,2},\mu| \le 1\,\mathrm{TeV}$; $100\,\mathrm{GeV} \le M_3 \le 1\,\mathrm{TeV}$; $|A_{b,t,\tau}| \le 1\,\mathrm{TeV}$; $1 \le \tan\beta \le 50$; $43.5\,\mathrm{GeV} \le m_A \le 1\,\mathrm{TeV}$. We randomly generated 10^7 points in this parameter space and subjected them to an exhaustive set of existing theoretical and experimental constraints. We also performed a similar scan with log priors (with slightly different mass ranges) to gauge the influence of priors on our results and found these to be negiglible[3]. We then generated SUSY spectra utilizing SuSpect2.34[2].

2. Theoretical and Experimental Constraints

We now discuss the theoretical and experimental constraints that we applied to the generated parameter space points; for more details, one should consult [3,4].

2.1. Theoretical Constraints

We demanded that the sparticle spectrum not have tachyons or color or charge breaking minima in the scalar potential and also required that the Higgs potential be bounded from below with consistent electroweak symmetry breaking. We

*Presented at the *Dark Matter Conference*, 9-11 Feb 2009, Arcetri, Florence, Italy. SLAC-PUB-13731. Work supported in part by the Department of Energy, Contract DE-AC02-76SF00515.

Work supported in part by US Department of Energy contract DE-AC02-76SF00515.

assume that the LSP, which will be absolutely stable, be a conventional thermal relic and identify the LSP as the lightest neutralino.

2.2. Low Energy Constraints

The code micrOMEGAs2.20[5] was used to evaluate the following observables for each point in the parameter space: $\Delta\rho$, the decay rates for $b \to s\gamma$ and $B_s \to \mu^+\mu^-$, and the $g-2$ of the muon. In addition, we evaluated the branching fraction for $B \to \tau\nu$ following[6] and [7]. We allowed a large range for the SUSY contribution to $g-2$ due to the evolving discrepancy between theory and experiment[8]. We implemented constraints from meson-antimeson mixing[9] by assuming MFV[1], imposing first and second generation mass degeneracy, and demanding that the ratio of first/second to third generation squark soft breaking masses differ from unity by no more than a factor of 5.

2.3. Accelerator Constraints

LEP data at the Z pole shows that charged sparticles with masses below $M_Z/2$ are unlikely. This also holds for the lightest neutral Higgs boson. Data from LEPII[10] indicates that there are no new *stable* charged particles of any kind with masses below 100 GeV. We also require that any new contributions to the invisible width of the Z boson be ≤ 2 MeV[11].

Results from sparticle searches at LEPII possess numerous caveats. We implement a lower limit of 92 GeV on first and second generation squark masses[12] and 95 GeV on the sbottom mass[13], provided that the gluino is more massive than the squarks and the mass difference (Δm) between the squark and the LSP is $\geq$ 10 GeV. We demand that the lightest stop mass be greater than 95(97) GeV[14] if the stop can(cannot) decay into $Wb\chi_1^0$. The right-handed sleptons must have masses greater than 100, 95, or 90 GeV for selectrons, smuons, and staus respectively, as long as the condition $0.97 m_{\rm slepton} > m_{\rm LSP}$ is satisfied. These bounds are also applied to left-handed sleptons, when the neutralino $t-$channel diagram may be neglected in the case of selectrons. Chargino masses be greater than 103(95) GeV, provided that the LSP-chargino mass splitting is $\Delta m > (<)2$ GeV[14]. If the lightest chargino is dominantly Wino, this limit only applies when the electron sneutrino $t-$channel diagram is negligible. The LEP Higgs Working Group[15], provides five sets of constraints on the MSSM Higgs sector, which are essentially limits on the Higgs-Z coupling times the Higgs branching fraction for various final states. We employ SUSY-HIT[16] to analyze these. In addition, we included a theoretical uncertainty on the calculated mass of the lightest Higgs boson of approximately 3 GeV[17] when applying these constraints.

We also employ constraints from searches at the Tevatron. Restrictions on the squark and gluino sectors arise from the null D0 multijet plus missing energy search[18]. We generalize their analysis, rendering it model independent, by generating multijet plus missing energy events for our models using PYTHIA6.4[19] as interfaced to PGS4 [20] which provides a fast detector simulation. We weigh our results with K factors computed using PROSPINO2.0 [21]. Analogously, we employ constraints from the CDF search for trileptons plus missing energy[22], which we also generalize to the full pMSSM. D0[23] has obtained lower limits on the mass of heavy stable charged particles. We take this constraint to be $m_{\chi^+} \geq 206|U_{1w}|^2 + 171|U_{1h}|^2$ GeV at 95% CL for charginos, where the matrix entries U_{1w} and U_{1h} determine the Wino/Higgsino content of the lightest chargino. CDF and D0 also have analyses that search for light stops and sbottoms[24]; these searches are difficult to implement in a model-independent pMSSM context and thus we exclude models with light ($m < m_t$) stops or sbottoms.

2.4. Astrophysical Constraints

There are two constraints from considering the LSP as a long-lived relic. As noted above, we demand that the LSP be the lightest neutralino. We also require, following the 5 year WMAP measurement[25] of the relic density, that $\Omega h^2|_{\rm LSP} \leq 0.121$. In not employing a lower bound on $\Omega h^2|_{\rm LSP}$ for our models, we acknowledge the possibility that even within the MSSM and the thermal relic framework, dark matter may have multiple components. However, in discussing re-

sults below, we will also examine a subset of models for which $0.100 \leq \Omega h^2|_{LSP} \leq 0.121$.

We also obtain constraints from direct dark matter searches[26]. Generally, the strongest constraints come from the spin-independent WIMP-nucleon cross sections, hence we only implement bounds on our models from these; inspection of the spin-dependent WIMP-nucleon cross sections in our models confirms that this approach is reasonable. Both spin-independent and spin-dependent cross sections were calculated using micrOMEGAs2.21[5]. We implement cross section limits from XENON10[27], CDMS[28], CRESST I[29] and DAMA[30] data. It should be noted that many of our models predict a value $\Omega h^2|_{\rm LSP}$ which is less than that observed by WMAP and supernova searches. We thus scale our cross sections to take this into account.

3. Results

As noted above, we randomly generated 10^7 parameter space points (*i.e.*, models) in a 19-dimensional pMSSM parameter space using flat priors. Only $\sim 68.5 \cdot 10^3$ of these models satisfy all the constraints listed above. The properties of these models are described in much greater detail in [3]. Here we will discuss the attributes of these models which are most important astrophysically.

Figure 1 presents a histogram of the masses of the four neutralino and two chargino species in our models. The lightest neutralino is, of course, the LSP. The LSP mass lies between 100 and 250 GeV in over 70% of our models. Generally models with a mostly Higgsino or Wino LSP have a chargino with nearly the same mass as the LSP; as sufficiently light charginos would normally have been detected at LEP or the Tevatron, there are fewer models with such LSPs with mass $\lesssim 100$ GeV.

The identity of the nLSP is shown in Figure 2. The lightest chargino is the nLSP in about 78% of the models; this is due to many models having Wino or Higgsino LSPs, and the generally small mass splitting between a mostly Wino or Higgsino neutralino and the corresponding chargino. The second lightest neutralino is the nLSP $\sim 6\%$ of the time. These will generally be models with a

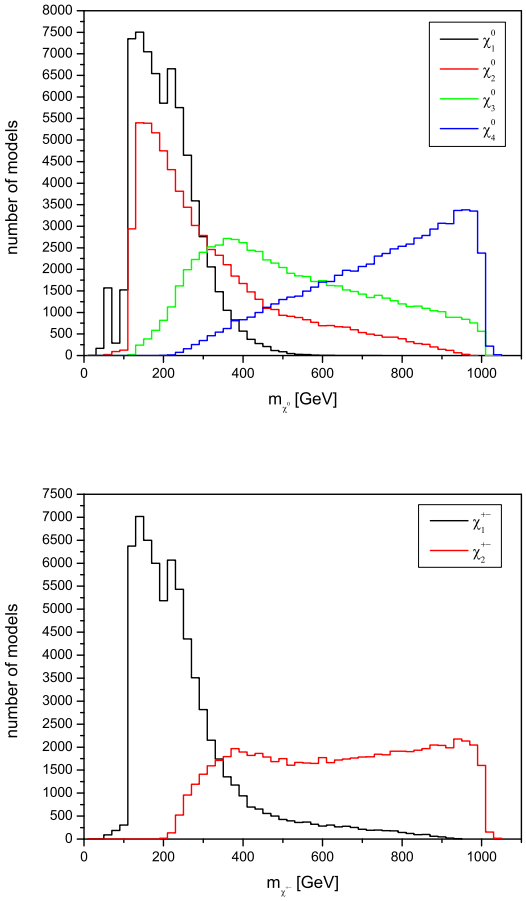

Figure 1. Distribution of neutralino masses (top panel) and chargino masses (bottom panel) for our set of models.

dominantly Higgsino LSP. Note also that while neutralinos or charginos are the nLSP in the vast majority of cases, there are 10 other sparticles each of which is the nLSP in $> 1\%$ of our models. Scenarios in which these sparticles are the nLSP may lead to interesting signatures at the LHC[31].

Figure 3 displays the LSP mass value as a function of the LSP-nLSP mass splitting, Δm, our models for each identity of the LSP. It is interesting that these models have a smaller Δm than is often considered; 80% of our models have $\Delta m < 10$ GeV, 27% have $\Delta m < 1$ GeV, and 3%

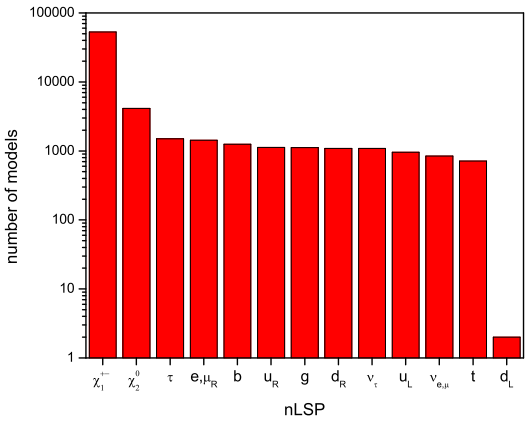

Figure 2. Number of models in which the nLSP is the given sparticle.

have $\Delta m < 10$ MeV. As one can see from Figure 3, this occurs largely, but not exclusively, in models with a chargino nLSP. This is again due to the many models where the LSP is nearly pure Wino or Higgsino.

There are a number of interesting features in this figure. The mostly empty square region which appears on the lower left-hand side of Figure 3 is due to the fact that models with chargino nLSPs in this mass and Δm range have been excluded by the Tevatron stable chargino search. Non-chargino nLSPs are not eliminated by this search (*e.g.*, the production cross section for sleptons in this range is too small to be excluded by the Tevatron search). It is perhaps worth noting that a stable heavy charged particle search at the LHC, corresponding to those done at the Tevatron, would be able to exclude or discover the models with heavier chargino nLSPs and small values of Δm (corresponding to $\sim$ 12% of our model set).

Another interesting feature in this figure is the bulge for 0.1 GeV $\leq \Delta m \lesssim 2$ GeV and $m_{LSP} \lesssim 100$ GeV. This region exists because these values of Δm are large enough that at LEP or the Tevatron, the produced chargino would decay in the detector, but the resulting charged tracks would be too soft to be observed. The existence of such a region shows the difficulty of making model independent statements about sparticle masses or other SUSY observables.

We have seen that within our model set the nLSP can be almost any SUSY particle and the corresponding Δm can be small for these cases. Thus specific models in our set describe qualitatively most of the conventional long-lived sparticle scenarios. Long-lived stops or staus (as in GMSB), gluinos (as in Split SUSY) as well as charginos (as in AMSB) all occur in our sample. We also have long-lived neutralinos, as does GMSB, however these are the $\tilde{\chi}_2^0$ in our case. In addition to models which, to some extent, correspond to these well-studied scenarios, we also have models with long-lived selectrons, sneutrinos and sbottoms.

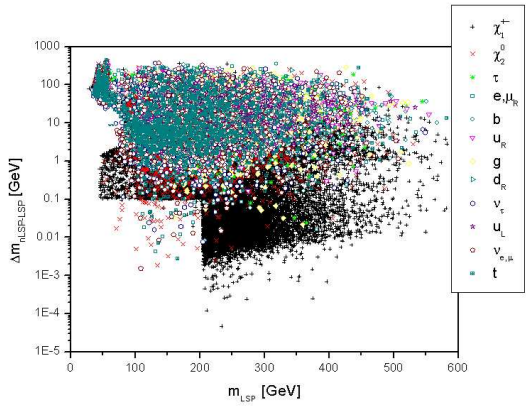

Figure 3. Mass splitting between nLSP and LSP versus LSP mass. The identity of the nLSP is shown as well. (The LSP is always the lightest neutralino in our set of models).

Figures 4, and 5 display the gauge eigenstate content of the LSPs in our model set. We note that most LSPs are relatively pure eigenstates, with models where the LSP is Higgsino or mostly Higgsino being by far the most common. About one quarter of our models have Wino or mostly Wino LSPs, while just over one-sixth have Bino or mostly Bino LSPs. Within mSUGRA, the LSP is, in general, nearly purely Bino; this suggests

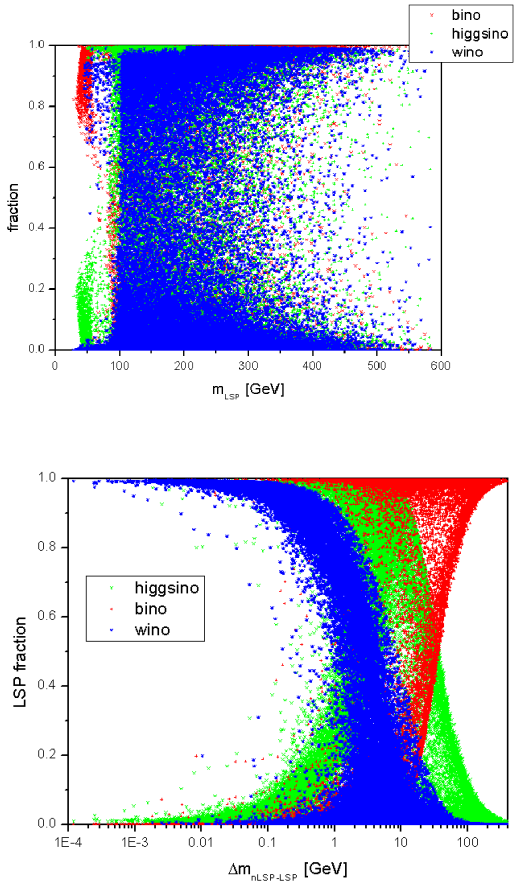

Figure 4. The distribution of LSP gaugino eigenstate types as a function of the LSP mass (top panel) or the LSP-nLSP mass difference (bottom panel). Note that each LSP corresponds to three points on this figure, one each for its Bino, Wino, and Higgsino fraction.

that most of our models are substantially different from mSUGRA. We note that one would expect the LSP be a pure eigenstate fairly often in a random scan of Lagrangian parameters, since if the differences between M_1, M_2, and μ are large compared to M_Z, then the eigenstates of the mixing matrix will be essentially pure gaugino and Higgsino states.

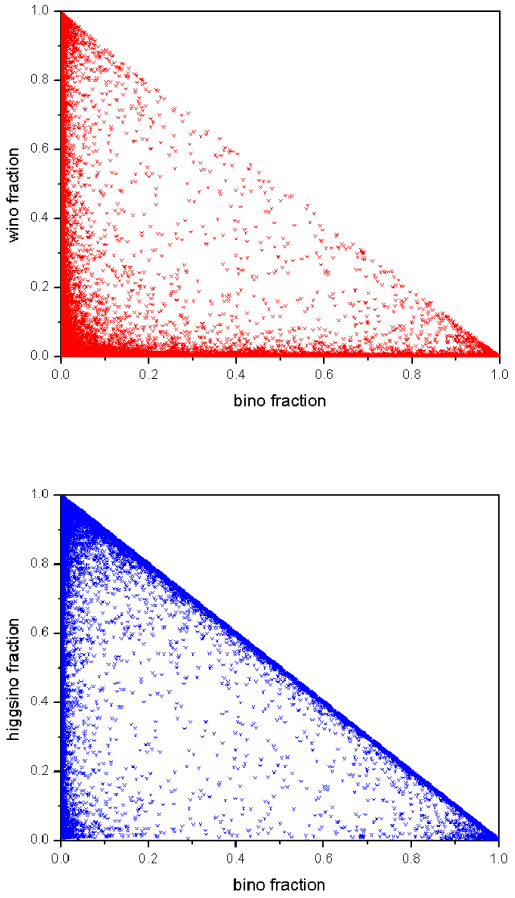

Figure 5. Wino/Higgsino/Bino content of the LSP in the case of flat priors. Note that, as elsewhere in the paper, $|Z_{11}|^2$, $|Z_{12}|^2$, and $|Z_{13}|^2 + |Z_{14}|^2$, where Z_{ij} is the neutralino mixing matrix, give the Bino, Wino, and Higgsino fractions respectively.

3.1. Relic Density

We did not demand that the LSP, in any given model, account for all of the dark matter, rather we required only that the LSP relic density not be too large to be consistent with WMAP. More specifically, we employed $\Omega h^2|_{\rm LSP} < 0.121$. Figure 6 shows the distribution of $\Omega h^2|_{\rm LSP}$ values predicted by our model set. Note that this distribution is peaked at small values of $\Omega h^2|_{\rm LSP}$. In particular, the mean value for this quantity in our models is ~ 0.012. We note that the range of possible values of $\Omega h^2|_{\rm LSP}$ is found to be much larger than those obtained by analyses of specific SUSY breaking scenarios[32]. We display the predictions for $\Omega h^2|_{\rm LSP}$ versus the LSP mass and versus the nLSP - LSP mass splitting in Figure 7. Figure 7 makes it clear that $\Omega h^2|_{\rm LSP}$ generally increases with the LSP mass, but a large range of values for the relic density are possible at any given LSP mass. The empty region in Figure 7 where $\Omega h^2|_{\rm LSP} \approx 0.001-0.1$ and $m_{\rm LSP} \approx 50-100$ is due to the fact that, in general, LSPs which are mostly Higgsino or Wino give lower values of $\Omega h^2|_{\rm LSP}$, and, as noted above, there are fewer Higgsino or Wino LSPs in this mass range. This figure also shows that small mass differences can lead to large dark matter annihilation rates.

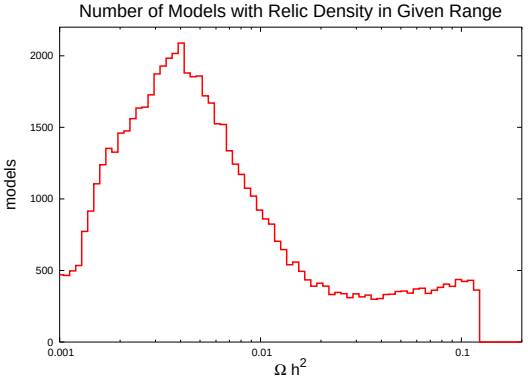

Figure 6. Distribution of $\Omega h^2|_{\rm LSP}$ for our models.

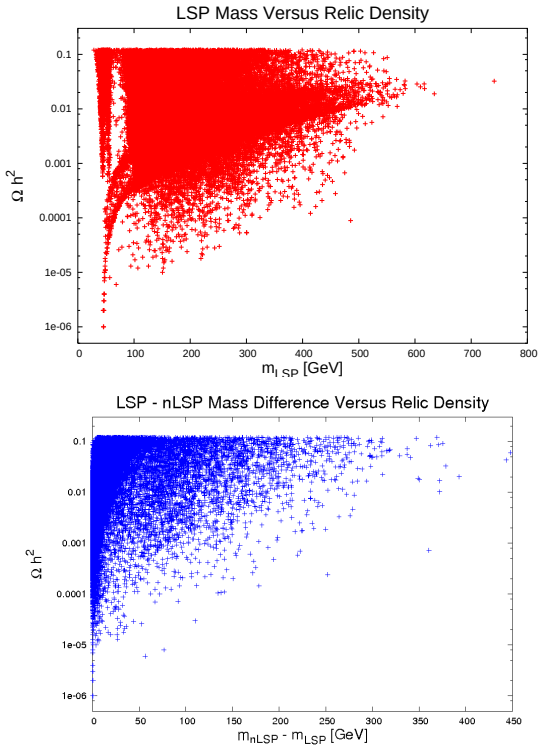

Figure 7. Distribution of $\Omega h^2|_{\rm LSP}$ as a function of the LSP mass (top panel) or the LSP-nLSP mass splitting (bottom panel.

3.2. Direct Detection of Dark Matter

As noted above, we calculate the spin-dependent and spin-independent WIMP-nucleon cross sections using micrOMEGAs 2.21 [5]. These data give the possible signatures in our model set for experiments that search for WIMPs directly. As these experiments measure the product of WIMP-nucleon cross sections with the local relic density, the cross section data presented in the figures below are scaled by $\xi = \Omega h^2|_{\rm LSP}/\Omega h^2|_{\rm WMAP}$. To date, these experiments generally provide a more significant bound on the spin-independent cross section, and hence we will focus on those.

Figure 8 presents the distribution for the scaled WIMP-proton spin-independent cross section versus relic density for our model sample. As one would expect, larger values of the cross

section are generally found at larger values of $\Omega h^2|_{\rm LSP}$. However, even for relic densities close to the WMAP value, $\xi\sigma_{p,SI}$ is seen to vary by almost eight orders of magnitude. These ranges for $\xi\sigma_{p,SI}$ are much larger than those from mSUGRA as calculated, *e.g.*, in [33].

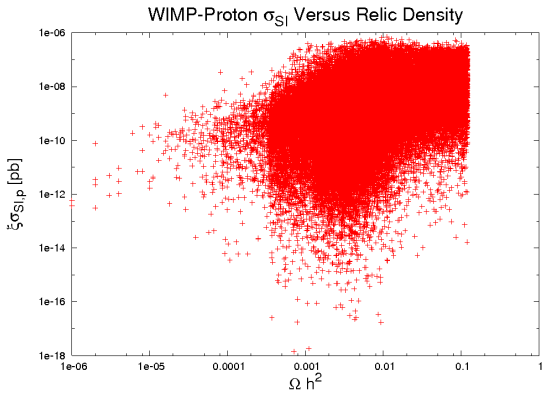

Figure 8. Distribution of scaled WIMP-proton spin-independent cross section versus the LSP contribution to relic density for our models.

Figure 9 shows the scaled WIMP-proton spin-dependent and spin-independent cross sections as a function of the LSP mass. The constraints from XENON10[27] and CDMS[28] are also displayed. As noted above, to take the uncertainties in the theoretical calculations of the WIMP-nucleon cross section into account, we allowed for a factor of 4 uncertainty in the calculation of the WIMP-nucleon cross section. Table 3 in Ref.[4] gives the fraction of models that would be excluded if the combined CDMS/XENON10 cross section limit were improved by an overall scaling factor. Note that our inclusion of the theoretical uncertainties does not significantly modify the size of our model sample.

We find that the range of values obtained for these cross sections covers the entire region in cross section/ LSP space that is anticipated from different types of Beyond the Standard Model theories in the above reference. This suggests

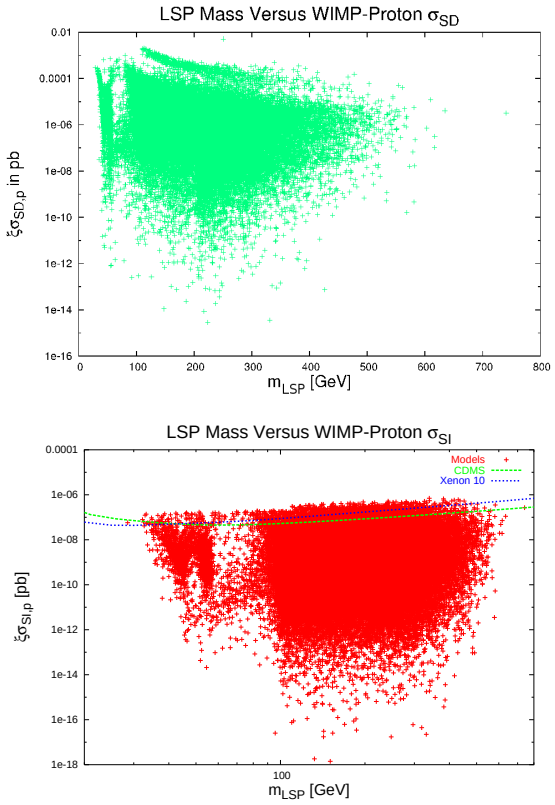

Figure 9. Distributions of scaled WIMP-proton spin-dependent cross section and spin-independent cross sections versus LSP mass in our models. In the spin-independent panel, the CDMS and Xenon10 bounds are shown.

that we cannot use direct detection experiments to distinguish between *e.g.* SUSY versus Little Higgs versus Universal Extra Dimensions dark matter candidates in the absence of other data.

In Figure 10, we compare the WIMP-proton and WIMP-neutron cross sections in the spin-dependent and spin-independent cases. The spin-independent cross sections are seen to be fairly isospin independent; this is not the case, however, for the spin-dependent cross sections.

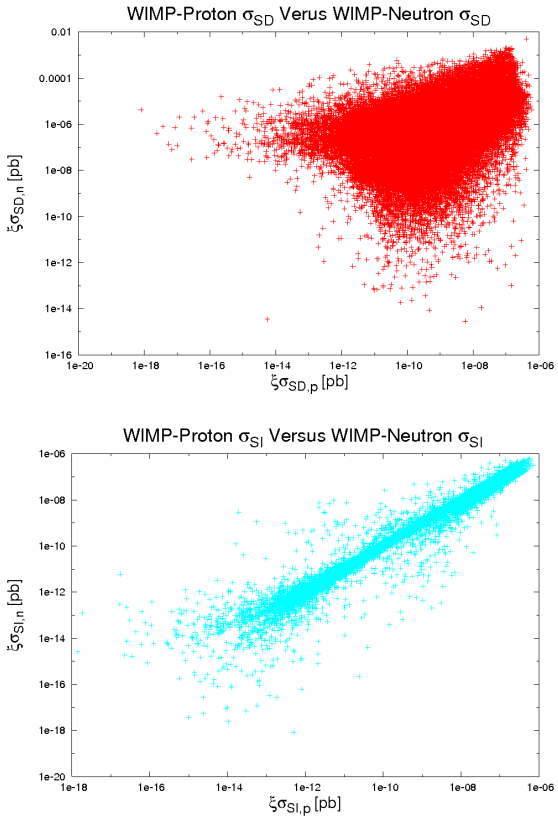

Figure 10. Comparison of the WIMP-neutron and WIMP-proton cross sections. The spin-dependent(independent) cross sections are shown in the top(bottom) panel.

3.3. Indirect Detection of Dark Matter

The PAMELA collaboration has recently claimed an excess in the ratio of cosmic ray positrons to electrons observed at energies $\gtrsim 10$ GeV[34]. Here we employ DarkSUSY 5.0.4[35] to calculate this ratio for our model sample and compare these results with the PAMELA data.

In general, for a thermal relic dark matter candidate to reproduce the PAMELA data, its signal rate must be multiplied by a boost factor[36]. In nature, such a boost factor could result from, *e.g.*, a local overdensity. The boost factor in that case would be the square of the ratio between the density of dark matter in the region from which one is sensitive to cosmic ray positrons and electrons to the universe as a whole.

In our analysis, we use four propagation models which are present in darkSUSY: the model of Baltz and Edsjö[37], that of Kamionkowski and Turner[38], that of Moskalenko and Strong[39], as well as GALPROP[40]. These are referred to in the following figures as "BE","KT","MS", and "GAL", respectively. Interestingly, we find that the extent to which the positron/electron flux ratio predicted by our models matches the PAMELA data can be highly sensitive to the choice of propagation model parameters. We will explore this further in future work[41].

The differential positron flux as a function of energy for a random sample of 500 models from our set are shown in Figure 11. Here we assume a boost factor of 1; the normalization of the curves takes into account the fact that for many of these models $\Omega h^2|_{\rm LSP} < \Omega_{\rm WMAP}$.

We next determine how well the predicted positron fluxes for these models agree with the PAMELA data, allowing for the possibility of a boost factor. To do this, we find the value for the boost factor (with the restriction that it be < 2000) which minimizes the χ^2 for the fit of each model's prediction to the PAMELA data. In calculating the χ^2, we consider only the seven highest energy bins, as at lower energies solar modulation is expected to play a major role[34]. Figure 12 shows the χ^2 and corresponding boost factor for these 500 random models. Note that there are four data points for each model, so there are actually 2000 data points in this figure. We then

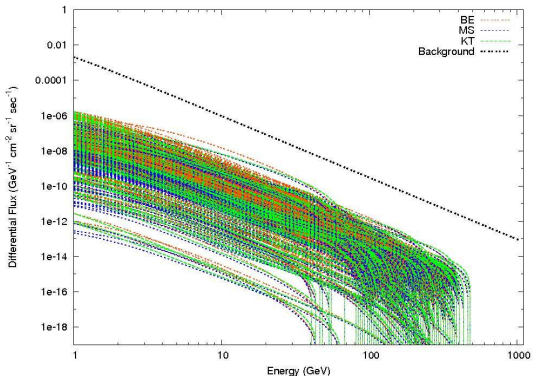

Figure 11. Expected flux spectrum of positrons from neutralino annihilation in the halo for 500 randomly selected models. For each model, there are three curves, one for each of three propagation models (as shown in the legend and defined in the text). The dotted black line is the expected background of positrons from non-SUSY processes.

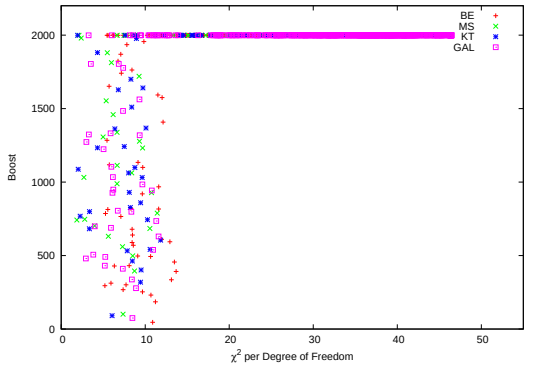

Figure 12. The distribution of χ^2 per degree of freedom versus the choice of boost factor that minimized this quantity for 500 randomly selected pMSSM models in our model set. These quantities have been determined for each of four propagation models. Only boost factors less than 2000 were considered; this explains the large number of models for which the χ^2-minimizing boost was 2000.

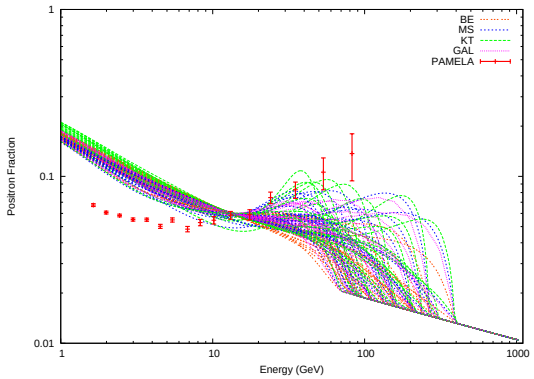

Figure 13. Positron/ electron flux ratio versus energy for the pMSSM models for which the χ^2 per degree of freedom with the χ^2-maximizing boost was less than 10.0 for three of the four propagation models. Curves are shown for all four propagation models.

display the positron to electron flux ratio, for the models with a low value of χ^2, as a function of energy in Figure 13, and note the reasonable agreement with the data for some models.

Since the flux from WIMP annihilation scales as $(\Omega h^2|_{\rm LSP}/\Omega h^2|_{\rm WMAP})^2$, we might expect to improve the match to the PAMELA data using models from our sample for which $\Omega h^2|_{\rm LSP} \approx \Omega h^2|_{\rm WMAP}$. To test this, we examine the predicted positron flux for 500 random models with $\Omega h^2|_{\rm LSP} > 0.100$; these fluxes are shown in Figure 14 with no boost factor. We then again find the boost factor that minimizes the χ^2 of the positron to electron flux ratios with respect to the seven highest energy PAMELA bins; these are shown in Figure 15. Here, we note that there are many more models for which the χ^2-minimizing value for the boost factor is < 2000 and there are many more points for which the χ^2 value is low. The positron to electron flux ratios for these models, including the boost factor, are shown in Figure 16.

It appears that some of our models do a reasonably good job of fitting the PAMELA positron data, especially in the case where $\Omega h^2|_{\rm LSP}$ lies fairly close to the WMAP value. For most models, describing the PAMELA data requires large

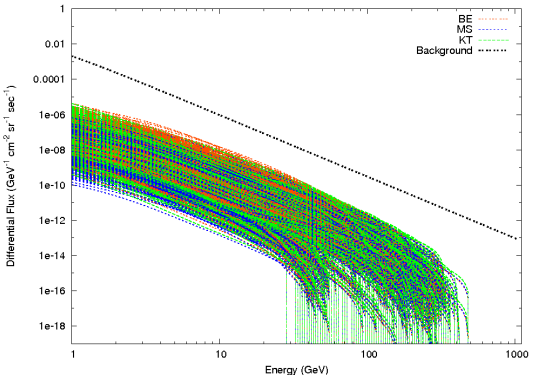

Figure 14. Expected flux spectrum of positrons from neutralino annihilation in the halo for 500 randomly selected models for which $\Omega h^2|_{\rm WMAP} \geq \Omega h^2|_{\rm LSP} > 0.10$. For each model, there are three curves, one for each of three propagation models (as shown in the legend). The dotted black line is the expected background of positrons from non-SUSY processes.

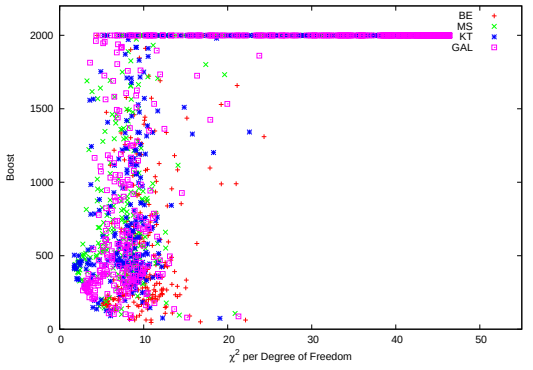

Figure 15. The distribution of χ^2 per degree of freedom versus the choice of boost factor that minimized this quantity for 500 randomly selected pMSSM models with $\Omega h^2|_{\rm WMAP} \geq \Omega h^2|_{\rm LSP} > 0.10$. These quantities have been determined for each of four propagation models. Only boost factors less than 2000 were considered; this explains the large number of models for which the χ^2-minimizing boost was 2000.

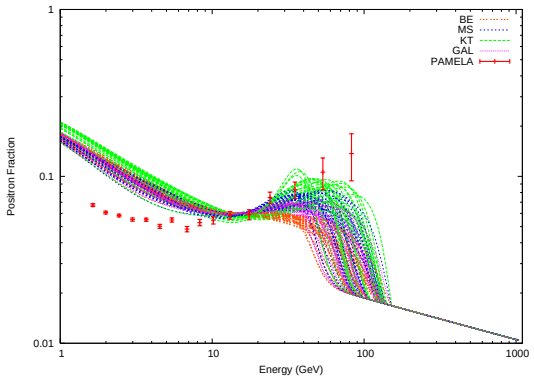

Figure 16. Positron/ electron flux ratio versus energy curves for pMSSM models for which the χ^2 per degree of freedom with the χ^2-maximizing boost was less than 5.0 for three of the four propagation models. Curves are shown for all four propagation models.

boost factors, however this is also a fairly generic feature of attempts to explain PAMELA and ATIC data in terms of WIMP annihilation[36]. There are however, many models which give relatively low χ^2 per degree of freedom in the fit to the data with relatively small boost factors. We will study this further in future work [41]. A study of the corresponding predictions for the the cosmic ray anti-proton flux is also underway.

4. Conclusions

We have generated a large set of points in parameter space (which we call "models") for the 19-parameter CP-conserving pMSSM, where MFV has been assumed. We subjected these models to numerous experimental and theoretical constraints to obtain a set of $\sim$ 68 K models which are consistent with existing data. We attempted to be somewhat conservative in our implementation of these constraints; in particular we only demanded that the relic density of the LSP not be greater than the measured value of Ωh^2 for non-baryonic dark matter, rather than assuming that the LSP must account for the *entire* observed relic density.

Examining the properties of the neutralinos in

these models, we find that many are relatively pure gauge eigenstates with Higgsinos being the most common, followed by Winos. The relative prevalence of Higgsino and Wino LSPs leads many of our models to have a chargino as nLSP, often with a relatively small mass splitting between this nLSP and the LSP; this has important consequences in both collider and astroparticle phenomenology.

We find that, in general, the LSP in our models provides a relatively small ($\sim 4\%$) contribution to the dark matter, however there is a long tail to this distribution and a substantial number of models for which the LSP makes up all or most of the dark matter. Typically these neutralinos are mostly Binos.

Examining the signatures of our models in direct and indirect dark matter detection experiments, we find a wide range of signatures for both cases. In particular, we find a much larger range of WIMP-nucleon cross sections than is found in any particular model of SUSY-breaking. As these cross sections also enter the regions of parameter space suggested by non-SUSY models, it appears that the discovery of WIMPs in direct detection experiments might not be sufficient to determine the correct model of the underlying physics. As a first look at the signatures of these models in indirect detection experiments, we examined whether our models could explain the PAMELA excess in the positron to electron ratio at high energies. We find that there are models which fit the PAMELA data rather well, and some of these have significantly smaller boost factors than generally assumed for a thermal relic.

The study of the pMSSM presents exciting new possibilities for SUSY phenomenology. The next few years will hopefully see important discoveries both in colliders and in satellite or ground-based astrophysical experiments. It is important that we follow the data and not our existing prejudices; hopefully this sort of relatively model-independent approach to collider and astrophysical phenomenology can be useful in this regard.

REFERENCES

1. For a review, see, G. D'Ambrosio, G. F. Giudice, G. Isidori and A. Strumia, Nucl. Phys. B **645**, 155 (2002) [arXiv:hep-ph/0207036].
2. A. Djouadi, J. L. Kneur and G. Moultaka, Comput. Phys. Commun. **176**, 426 (2007) [arXiv:hep-ph/0211331].
3. C. F. Berger, J. S. Gainer, J. L. Hewett and T. G. Rizzo, JHEP **0902**, 023 (2009) [arXiv:0812.0980 [hep-ph]].
4. R. C. Cotta, J. S. Gainer, J. L. Hewett and T. G. Rizzo, arXiv:0903.4409 [hep-ph].
5. G. Belanger, F. Boudjema, A. Pukhov and A. Semenov, Comput. Phys. Commun. **177** (2007) 894; arXiv:0803.2360 [hep-ph]; Comput. Phys. Commun. **149**, 103 (2002) [arXiv:hep-ph/0112278]; Comput. Phys. Commun. **174**, 577 (2006) [arXiv:hep-ph/0405253]; Comput. Phys. Commun. **176**, 367 (2007) [arXiv:hep-ph/0607059] and arXiv:0803.2360 [hep-ph].
6. G. Isidori and P. Paradisi, Phys. Lett. B **639**, 499 (2006) [arXiv:hep-ph/0605012].
7. D. Eriksson, F. Mahmoudi and O. Stal, arXiv:0808.3551 [hep-ph].
8. G. W. Bennett *et al.* [Muon G-2 Collaboration], Phys. Rev. D **73**, 072003 (2006) [arXiv:hep-ex/0602035].
9. For an introduction, see, J. S. Hagelin, S. Kelley and T. Tanaka, Nucl. Phys. B **415**, 293 (1994); F. Gabbiani *et al.*, Nucl. Phys. B **477**, 321 (1996) [arXiv:hep-ph/9604387].
10. G. Benelli, "Search for stable and long lived heavy charged particles in electron positron collisions at center of mass energies from 130-GeV to 209-GeV with the OPAL detector at LEP," UMI-31-09638, 2003. 126pp.
11. LEP Electroweak Working Group, http://www.cern.ch/LEPEWWG.
12. R. Barate *et al.* [ALEPH Collaboration], Phys. Lett. B **469**, 303 (1999).
13. A. C. Kraan, arXiv:hep-ex/0305051.
14. LEP SUSY Working Group, http://lepsusy.web.cern.ch/lepsusy/.
15. LEP Higgs Working Group, http://lephiggs.web.cern.ch/LEPHIGGS/

www/Welcome.html.
16. A. Djouadi, M. M. Muhlleitner and M. Spira, Acta Phys. Polon. B **38**, 635 (2007) [arXiv:hep-ph/0609292]; http://lappweb.in2p3.fr/~tmuehlleitner/SUSY-HIT/.
17. For a review, see, for example, S. Heinemeyer, W. Hollik and G. Weiglein, Phys. Rept. **425**, 265 (2006) [arXiv:hep-ph/0412214].
18. V. M. Abazov *et al.* [D0 Collaboration], Phys. Lett. B **660**, 449 (2008) [arXiv:0712.3805 [hep-ex]].
19. T. Sjostrand, S. Mrenna and P. Skands, JHEP **0605**, 026 (2006) [arXiv:hep-ph/0603175].
20. J. Conway, PGS4, Pretty Good detector Simulation, http://www.physics.ucdavis.edu/~conway/research/software/pgs/pgs.html.
21. W. Beenakker, R. Hopker and M. Spira, arXiv:hep-ph/9611232; W. Beenakker, R. Hopker, M. Spira and P. M. Zerwas, Nucl. Phys. B **492**, 51 (1997) [arXiv:hep-ph/9610490]. See also, http://www.ph.ed.ac.uk/~tplehn/prospino/.
22. T. Aaltonen *et al.* [CDF Collaboration], arXiv:0808.2446 [hep-ex].
23. V. M. Abazov *et al.* [D0 Collaboration], arXiv:0809.4472 [hep-ex].
24. T. Aaltonen *et al.* [CDF Collaboration], Phys. Rev. Lett. **101**, 071802 (2008) [arXiv:0802.3887 [hep-ex]] and T. Aaltonen *et al.* [CDF Collaboration], Phys. Rev. D **76**, 072010 (2007) [arXiv:0707.2567 [hep-ex]]; V. M. Abazov *et al.* [D0 Collaboration], Phys. Rev. Lett. **97**, 171806 (2006) [arXiv:hep-ex/0608013] and Phys. Lett. B **665**, 1 (2008) [arXiv:0803.2263 [hep-ex]];
25. E. Komatsu *et al.* [WMAP Collaboration], arXiv:0803.0547 [astro-ph].
26. For a recent overview see J. D. Vergados, Lect. Notes Phys. **720**, 69 (2007) [arXiv:hep-ph/0601064].
27. U. Oberlack [XENON Collaboration], J. Phys. Conf. Ser. **110**, 062020 (2008).
28. Z. Ahmed *et al.* [CDMS Collaboration], arXiv:0802.3530 [astro-ph].
29. M. Bravin *et al.* [CRESST-Collaboration], Astropart. Phys. **12**, 107 (1999) [arXiv:hep-ex/9904005].
30. R. Bernabei *et al.* [DAMA Collaboration], Phys. Lett. B **480**, 23 (2000).
31. J. A. Conley, J. S. Gainer, J. L. Hewett, and T. G. Rizzo. In preparation.
32. There have been many such a analyses; a few recent representative examples are: B. C. Allanach, M. J. Dolan and A. M. Weber, JHEP **0808**, 105 (2008) [arXiv:0806.1184 [hep-ph]]; O. Buchmueller *et al.*, arXiv:0808.4128 [hep-ph]; R. Trotta, F. Feroz, M. P. Hobson, L. Roszkowski and R. R. de Austri, arXiv:0809.3792 [hep-ph]; U. Chattopadhyay and D. Das, arXiv:0809.4065 [hep-ph]; S. Heinemeyer, X. Miao, S. Su and G. Weiglein, arXiv:0805.2359 [hep-ph]; J. R. Ellis, S. Heinemeyer, K. A. Olive, A. M. Weber and G. Weiglein, JHEP **0708**, 083 (2007) [arXiv:0706.0652 [hep-ph]];
33. V. Barger, W. Y. Keung and G. Shaughnessy, arXiv:0806.1962 [hep-ph].
34. O. Adriani *et al.*, arXiv:0810.4995 [astro-ph].
35. P. Gondolo, J. Edsjö, P. Ullio, L. Bergstrom, M. Schelke and E. A. Baltz, JCAP **0407**, 008 (2004) [arXiv:astro-ph/0406204]. P. Gondolo, J. Edsj, P. Ullio, L. Bergstrm, M. Schelke, E.A. Baltz, T. Bringmann and G. Duda, http://www.physto.se/~edsjo/darksusy.
36. This is a fairly generic result, see for example: M. Cirelli, M. Kadastik, M. Raidal and A. Strumia, arXiv:0809.2409 [hep-ph]. I. Cholis, L. Goodenough, D. Hooper, M. Simet and N. Weiner, arXiv:0809.1683 [hep-ph]. D. Hooper and K. Zurek, arXiv:0902.0593 [hep-ph].
37. E. A. Baltz and J. Edsjö, Phys. Rev. D **59**, 023511 (1999) [arXiv:astro-ph/9808243].
38. M. Kamionkowski and M. S. Turner, Phys. Rev. D **43**, 1774 (1991). M. S. Turner and F. Wilczek, Phys. Rev. D **42**, 1001 (1990).
39. I. V. Moskalenko and A. W. Strong, Phys. Rev. D **60**, 063003 (1999) [arXiv:astro-ph/9905283].
40. http://galprop.stanford.edu/web_galprop/galprop_home.html.
41. R. C. Cotta, J. S. Gainer, J. L. Hewett, and T. G. Rizzo. In preparation.